Analytical and Bioanalytical Chemistry (2021) 413:1405–1415
https://doi.org/10.1007/s00216-020-03104-7

RESEARCH PAPER

Sensitive ratiometric fluorescence assay for detecting xanthine in serum based on the inner filter effect of enzyme-catalyzed oxidation products to silicon nanoparticles

Dan Li[1] · Fangfang Chen[2] · Na Li[3] · Xiwen Ye[1] · Ying Sun[1] · Pinyi Ma[1] · Daqian Song[1] · Xinghua Wang[1]

Received: 28 March 2020 / Revised: 22 November 2020 / Accepted: 30 November 2020 / Published online: 2 January 2021
© Springer-Verlag GmbH Germany, part of Springer Nature 2021

Abstract

A new type of fluorescent silicon nanoparticles (SiNPs) were prepared via a facile one-pot hydrothermal method by using *N*-[3-(trimethoxysilyl)propyl]-ethylenediamine (DAMO) and glucose as reagents, and were subsequently applied to construct a ratiometric fluorescence assay for sensitive and rapid determination of xanthine in human serum. Two catalytic oxidation reactions were employed to induce a fluorescence response of the testing system towards xanthine. Under the catalysis of xanthine oxidase (XOD), xanthine in serum samples was oxidized and produced hydrogen peroxide (H_2O_2). By utilizing *o*-phenylenediamine (OPD) as the substrate for horseradish peroxidase (HRP) in the presence of H_2O_2, fluorescent 2,3-diaminophenazine (DAP) was finally generated. A ratiometric fluorescence assay for xanthine was established by determining the ratio of the green-yellow fluorescence emission of DAP and the blue fluorescence emitted from SiNPs under the inner filter effect (IFE) of DAP. Instead of traditional multi-step procedures for adding reacting reagents to the testing solution, all the reaction reagents were mixed with serum samples in a single step for this assay to shorten the total reaction time. This assay demonstrates superiority over a solo DAP fluorescence-based assay as well as other reported methods, with excellent sensitivity and reduced testing time. The strategies proposed in this work for both synthesis and application of fluorescent SiNPs can be used in future fabrication of novel fluorescent probes, especially for sensing biological metabolites involved in H_2O_2-generation or consumption reactions.

Keywords Xanthine · Hydrogen peroxide (H_2O_2) · Silicon nanoparticles (SiNPs) · Hydrothermal synthesis · Ratiometric fluorometry

Introduction

Xanthine is an intermediate of purine metabolism in the human body. It can be transformed to uric acid by the catalysis of xanthine oxidase (XOD) during the degradation progress of purine, and accordingly, it can be used as an indicator of abnormal purine levels. An elevated level of xanthine in plasma or urine has been associated with many diseases including gout, xanthinuria, hyperuricemia, cerebral ischemia, renal failure, pre-eclampsia, and urologic cancers [1–3]. Additionally, the xanthine level is regarded as a standard of freshness of fish meat due to the natural increase in xanthine content in meat with time elapsed after the death of fish [4]. Therefore, establishing sensitive, rapid and reliable analytical methods for monitoring of xanthine is of great importance for both clinical diagnostics and food safety.

Routine methods for determining xanthine include electrochemistry [5], colorimetry [6], capillary electrophoresis [7], high-performance liquid chromatography (HPLC) [3, 8], surface plasmon resonance [9], and fluorometry [10, 11]. Among these methods, fluorometry can provide balanced sensitivity, specificity, and convenience for sensing of biomaterials,

✉ Na Li
dreamerlina@163.com

✉ Xinghua Wang
starred.wang@gmail.com

[1] College of Chemistry, Jilin University, Qianjin Street 2699, Changchun 130012, Jilin, China

[2] Key Laboratory of Zoonoses Research, Ministry of Education, Nanomedicine and Translational Research Center, China-Japan Union Hospital of Jilin University, Changchun 130033, Jilin, China

[3] School of Information and Optoelectronic Science and Engineering, South China Normal University, Guangzhou 510006, Guangdong, China

especially after combination with fluorescent nanomaterials such as carbon dots (CDs) [12, 13]. Fluorescent silicon nanoparticles (SiNPs), as a type of newly emerged nanomaterials possessing superior quantum yield, excellent photostability, low cytotoxicity, and size-tunable emission wavelength [14–16], are regarded as promising alternatives to organic dyes, semiconductor quantum dots (QDs), and CDs. Theoretically, the superior quantum yield of SiNPs would benefit the sensitivity of fluorescent probes. However, reports of the synthesis and application of fluorescent SiNPs for bioanalysis or clinical diagnosis to date are rare [17, 18].

Compared with direct or quenching fluorometry, ratiometric fluorometry possesses the ability to eliminate spectral effects arising from the variability in measuring conditions, as well as to enhance a variety of signals, by simultaneously recording two measurable fluorescence signals at one excitation wavelength [9], which greatly improves the sensitivity of the related fluorescent probes. The inner filter effect (IFE) is common in fluorescence spectroscopy, and is mainly induced by the overlap between the absorption band of a certain substance and the excitation or emission bands of a fluorophore, and will result in the quenching of fluorescence emitted from the fluorophore. Therefore, IFE can also be utilized for the determination of the quencher as with other quenching effects [19].

In this work, we established a sensitive assay for serum xanthine based on fluorescent SiNPs by using an enzyme-triggered IFE and ratiometric fluorometry for the first time. During the assay, hydrogen peroxide (H_2O_2) was generated by the oxidation of xanthine with the catalysis of xanthine oxidase (XOD) after the one-step mixing of XOD, *o*-phenylenediamine (OPD), and horseradish peroxidase (HRP) as testing reagents with a serum sample. Oxidation of OPD was then induced by H_2O_2 under the catalysis of HRP, resulting in the production of 2,3-diaminophenazine (DAP). DAP emitted a green-yellow fluorescence at 560 nm, and suppressed the blue fluorescence emission of SiNPs at 425 nm by absorbing this emission via IFE. The ratios of fluorescence intensities at the above wavelengths (I_{560}/I_{425}) were calculated for constructing the concentration calibration line of xanthine. The excellent analytical performance of the proposed assay, including high sensitivity and short testing time, indicates its potential for sensitive and rapid determination of xanthine. Real and spiked human serum samples were examined by the proposed assay and, for comparison, by a solo DAP fluorescence-based assay that is commonly used in routine enzyme-linked fluorescence assay (ELFA). The good agreement between the results obtained by these assays demonstrates the applicability of the proposed assay. The mechanism of the IFE employed in this assay (Scheme 1) was confirmed by ultraviolet-visible (UV-Vis) absorption spectroscopy, fluorescence lifetime measurements, and corrected fluorescence spectra.

Experimental section

Materials and instruments

N-[3-(Trimethoxysilyl)propyl]-ethylenediamine (DAMO), glucose, and xanthine oxidase were obtained from Beijing J&K Chemicals. Xanthine, horseradish peroxidase (HRP), *o*-phenylenediamine (OPD), uric acid (UA), ascorbic acid (AA), galactose (Gal), and 3,3′,5,5’-tetramethylbenzidine (TMB) were

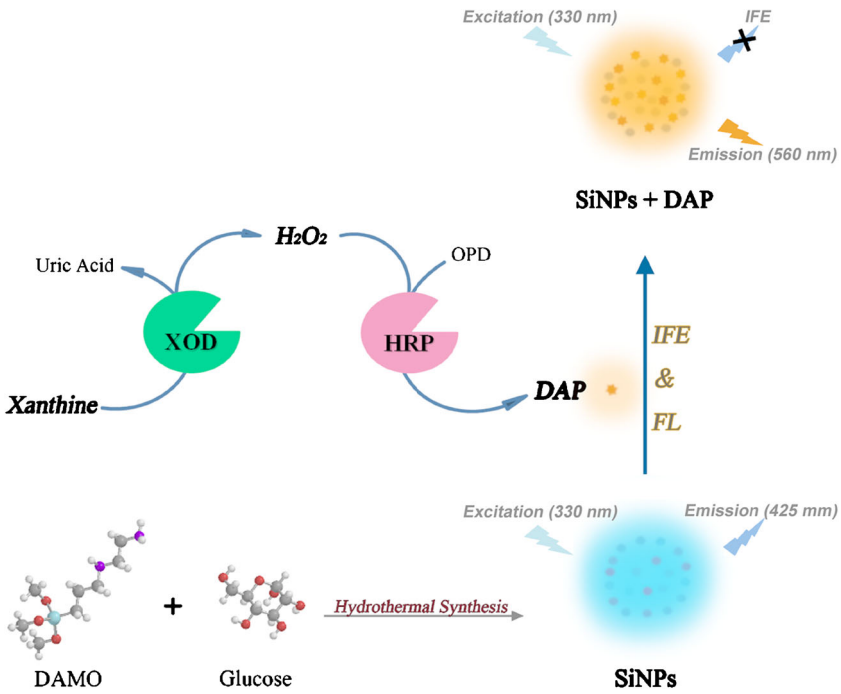

Scheme 1 Mechanism for xanthine sensing by means of the present assay

purchased from Shanghai Aladdin Industrial Corporation. Tyrosine (Tyr), L-cysteine (L-Cys), lysine (Lys), glutathione (GSH), acid phosphatase (ACP), transglutaminase (TG), glutamic-pyruvic transaminase (GPT), and human serum albumin (HSA) were from Shanghai Yuanye Bio-Technology Co., Ltd. A commonly used inhibitor of alkaline phosphatase (ALP), sodium orthovanadate (Na_3VO_4), was supplied by Shanghai Macklin Biochemical Technology Corporation. H_2O_2 (30%) was obtained from Beijing Chemical Works. Ultrapure water with resistivity of 18.25 MΩ·cm was prepared using a Milli-Q system (Millipore, USA). Xanthine aqueous solutions at various concentrations and OPD aqueous solutions were freshly prepared before use. HRP and XOD solutions were freshly prepared with phosphate buffer (PB, 10 mM, pH = 6.6) before use. Whole blood samples were taken at China-Japan Union Hospital of Jilin University (Changchun, China) from volunteers after physical examination and obtaining informed consent, with the permission of the hospital authority and the institutional ethics committee. Human serum samples were clotted for 2 h at room temperature, and then pooled and stored at −80 °C. Recovery experiments were performed with spiked serum samples.

A JEOL JEM-2100F transmission electron microscope (TEM, Japan) was used to characterize the morphology of the SiNPs. X-ray photoelectron spectroscopy (XPS) of the SiNPs was carried out with a Thermo ESCALAB 250 spectrometer (USA). A Thermo Nicolet Avatar 360 Fourier transform infrared (FT-IR) spectrometer (USA), a Hitachi F-2700 fluorescence spectrophotometer (Japan), and an Agilent Cary 60 UV-Vis spectrometer (USA) were respectively used to record infrared absorption spectra, fluorescence spectra, and UV-Vis absorption spectra. Fluorescence lifetime measurements were performed by a Horiba Jobin Yvon Fluorolog-3 spectrofluorometer (USA) equipped with a 455 nm NanoLED excitation source and a time-correlated single-photon counting unit. The pH values of all buffer solutions were confirmed by a Sartorius PB-10 pH meter (Germany). A Taisite electric oven (China) was employed during the hydrothermal reaction process.

Synthesis of SiNPs

Blue-emitting fluorescent SiNPs were synthesized by a facile one-pot hydrothermal strategy using DAMO and glucose as the organosilane source and the reducing agent, respectively. Briefly, 1 mL of DAMO was added to 5 mL of glucose aqueous solution (15 mg/mL). After mixing thoroughly, the solution was transferred into a 10 mL Teflon-lined autoclave, which was placed in an oven at 210 °C for 12 h for hydrothermal reactions. Next, the originally synthesized SiNPs were dialyzed with molecular weight cutoff of 1000 Da against ultrapure water for 5 h. Finally, the purified SiNPs were stored at 4 °C in the dark. Before the testing experiments, the SiNPs were diluted 250-fold with PB (10 mM, pH = 6.6).

Ratiometric fluorescence assay for H_2O_2

A series of standard H_2O_2 aqueous solutions at concentrations ranging from 0.1 to 1000 μM were freshly prepared. For detecting H_2O_2, 200 μL of each standard solution was mixed with 100 μL of PB (200 mM, pH = 6.6) in a 1.5 mL microcentrifuge tube. Then, testing reagents including 100 μL of OPD (20 mM), 50 μL of HRP (0.5 mg/mL), and 50 μL of SiNPs were added to the tube. After mixing thoroughly, the mixture was incubated at 37 °C in the dark for 30 min. Finally, the fluorescence spectrum of the mixture was collected under excitation of 330 nm at room temperature. The ratio of fluorescence intensities at 560 nm and 425 nm (I_{560}/I_{425}) was calculated for quantitation of H_2O_2. All experiments were carried out in triplicate.

Ratiometric fluorescence assay for xanthine

The procedure for the assay of xanthine in a standard solution or a serum sample was similar to that for H_2O_2, except for the employment of 50 μL of XOD (0.2 mg/mL) as an additional testing reagent. All experiments were carried out in triplicate.

Results and discussion

Characteristics of synthesized SiNPs

As shown in Fig. 1, the as-prepared SiNPs exhibited a monodisperse spherical morphology with an average diameter of 4.8 ± 0.78 nm (Fig. 1b). The identification of surface functional groups of the SiNPs was performed by FT-IR spectroscopy (Fig. 2a). Three narrow bands appeared at 1315 cm^{-1} and 1139–1036 cm^{-1}. The first was ascribed to the Si–C asymmetric deformation, and the latter two were associated with the Si–O–Si stretching vibration [16]. The band at 928 cm^{-1} was attributed to the Si–O stretching vibration of the Si–O–H group [20]. Two obvious absorption bands at 3424 cm^{-1} and 1648 cm^{-1} were respectively attributed to the stretching vibrations of the O–H and C=O groups [21, 22]. The unsaturated stretching vibration and the bending vibration of C–H presented characteristic absorption peaks at 2933 cm^{-1} and 1489 cm^{-1} [23], respectively. The characteristic absorption bands of the bending and wagging vibrations of N–H appeared at 1586 cm^{-1} and 779 cm^{-1} [24]. A weak band appearing at 1350 cm^{-1} was assigned to the C–N stretching vibration and the band at 694 cm^{-1} was attributed to a secondary amine [20]. These typical bands suggested that the surface of the as-prepared SiNPs was covered with abundant hydroxyl and amino groups, which provided good hydrophilicity and effective dispersion of the SiNPs in aqueous solution.

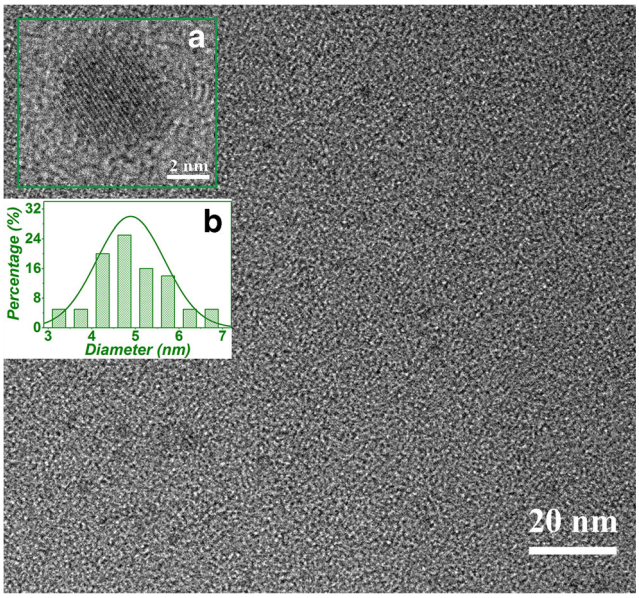

Fig. 1 TEM image of SiNPs. Inset is (**a**) lattice fringes and (**b**) size distribution of SiNPs

To further verify the surface functional group types, the XPS spectra of the SiNPs were recorded and analyzed. Five peaks shown in the full scan survey (Fig. 2b) at 102, 153, 284, 399, and 532 eV respectively represented Si 2p, Si 2s, C 1s, N 1s, and O 1s [23]. The chemical states of silicon were described by three peaks (Fig. 2c), which were Si–C (101.3 eV), Si–N (101.9 eV), and Si–O (102.5 eV) [24]. As shown in Fig. 2d, there were five peaks of C 1s at 284 eV, 284.6 eV, 285.2 eV, 286 eV, and 288.4 eV, corresponding to the C–Si, C–C/C=C, C–N, C–OH/C–O–C, and C=O groups, respectively [25]. The raw data spectrum of O 1s was fitted with three components (Fig. 2e), which were C=O (531 eV), Si–O (533.3 eV), and C–O (531.9 eV) [20, 26, 27]. As shown in Fig. 2f, there were three types of nitrogen atoms. The first two (398.4 eV and 399 eV) were attributed to Si–N and C–N groups, while the last (400 eV) was attributed to the C–$(N)_3$ group [23]. These results were consistent with those obtained by FT-IR.

The optical properties of the SiNPs were investigated by analyzing the corresponding spectra of UV-Vis absorption and fluorescence. UV-Vis absorption band at ~330 nm (Fig. 3a) was considered to arise from the trapping of excited-state energy by the surface defects of the SiNPs [28]. The SiNPs presented strong fluorescence emission at ~425 nm under excitation of 330 nm. Moreover, the peak emission wavelength of the fluorescence changed very little as the excitation wavelength varied in the range of 300 nm to 380 nm (Fig. 3b), demonstrating the largely size-independent emission characteristics of the SiNPs. The stability against photobleaching and the salt-tolerance performance of the SiNPs were tested in sequence (Fig. 3c, d). Results showed that irradiation at 425 nm for 60 min or dispersion in 100 mM NaCl solution had very little influence on the fluorescence emission of the SiNPs. As described in the Supplementary Information, the fluorescence quantum yield (QY) of the SiNPs evaluated in an aqueous solution was ~16%, which was higher than that of similar SiNPs synthesized using DAMO and catechol in our recent work (~11.1%) [18] or using glucose and (3-aminopropyl)trimethoxysilane (APTMS) in previously reported literature (~ 3.1%) [29]. As is well known, a higher QY value of a fluorescent material benefits its fluorescence response, resulting in improved sensitivity of its related fluorescence assay. There are two possible reasons for the production of the higher QY value in this work. One is the use of DAMO as the silicon source. DAMO

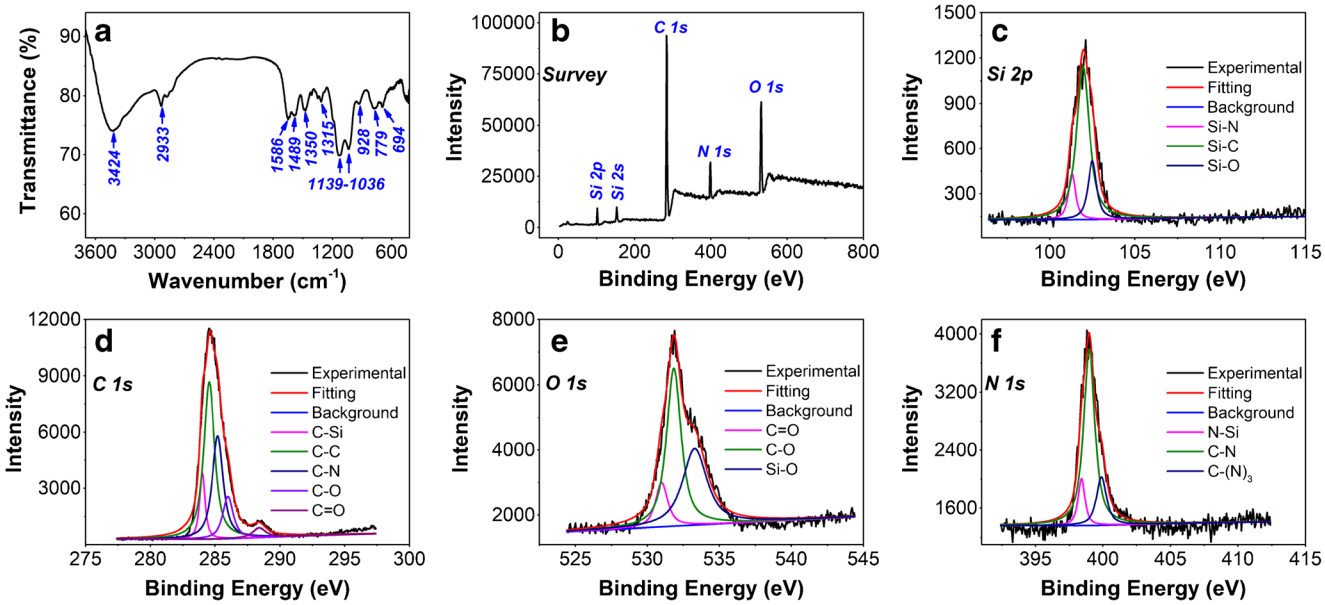

Fig. 2 **a** FT-IR spectrum of SiNPs. High-resolution XPS spectra of SiNPs: **b** full range, **c** Si 2p, **d** C 1s, **e** O 1s, and **f** N 1s

has a higher element ratio of N to Si than APTES, providing an appropriate proportion of doped N in the synthesized SiNPs to reduce the band gap energy. The other is the employment of a hydrothermal approach for synthesis. Hydrothermal synthesis improves the production of high-quality crystals and nanoparticles with uniform distribution.

Mechanism for sensing xanthine

The mechanism of the present assay for sensing xanthine can be regarded as both the fluorescence emission of DAP and the IFE of DAP on the fluorescence emitted from the SiNPs. Here, DAP is the final product of the two continuous catalytic oxidation reactions during assay, in which H_2O_2 is both the product of the former and the reactant of the latter.

As shown in Fig. 4a, OPD exhibited no obvious absorbance peak in the presence of H_2O_2 or HRP individually, but an extraordinary absorbance enhancement at 420 nm and remarkable fluorescence emission at 560 nm emerged when both H_2O_2 and HRP coexisted with OPD, revealing that OPD is oxidized to DAP by H_2O_2 under the catalysis of HRP. Nevertheless, there was an obvious overlap between the absorption band of DAP at 420 nm and the fluorescence emission band of the SiNPs at 425 nm, which showed that the production of DAP induces a large decrease in the fluorescence emitted from the SiNPs via the IFE. Therefore, by utilizing H_2O_2 generated from the catalytic oxidation of xanthine as the oxidant for the subsequent catalytic oxidation of OPD, fluorescence signals varying in an opposite manner at 560 nm and 425 nm towards xanthine would be observed. In this assay, the ratio of fluorescence intensities at 560 nm and 425 nm (I_{560}/I_{425}) was used as the response signal for determining xanthine.

The influence of solo OPD, H_2O_2, and HRP on the I_{560}/I_{425} values was examined individually (Fig. 4b). Results showed that the influence of these substrates was not obvious. However, the generation of DAP by mixing OPD, H_2O_2, and HRP together influenced the value of I_{560}/I_{425} significantly, which was in agreement with the mechanism proposed above.

It was observed that the fluorescence emission of the SiNPs gradually decreased with the continuous increase of DAP concentration (Fig. 4c). To further investigate the quenching process, the fluorescence decay of the SiNPs at 425 nm was measured firstly in various concentrations of DAP (Fig. 4d and Electronic Supplementary Material [ESM] Table S1). As is well known, the common dynamic quenching effect (DQE) induced by quencher molecules reduces the fluorescence lifetime of fluorophores by promoting the non-radiative energy transfer between excited-state fluorophores and matrix [30]. The very small variations in the fluorescence lifetime values obtained in this work clearly indicate that the DQE demonstrated almost no contribution to the quenching process.

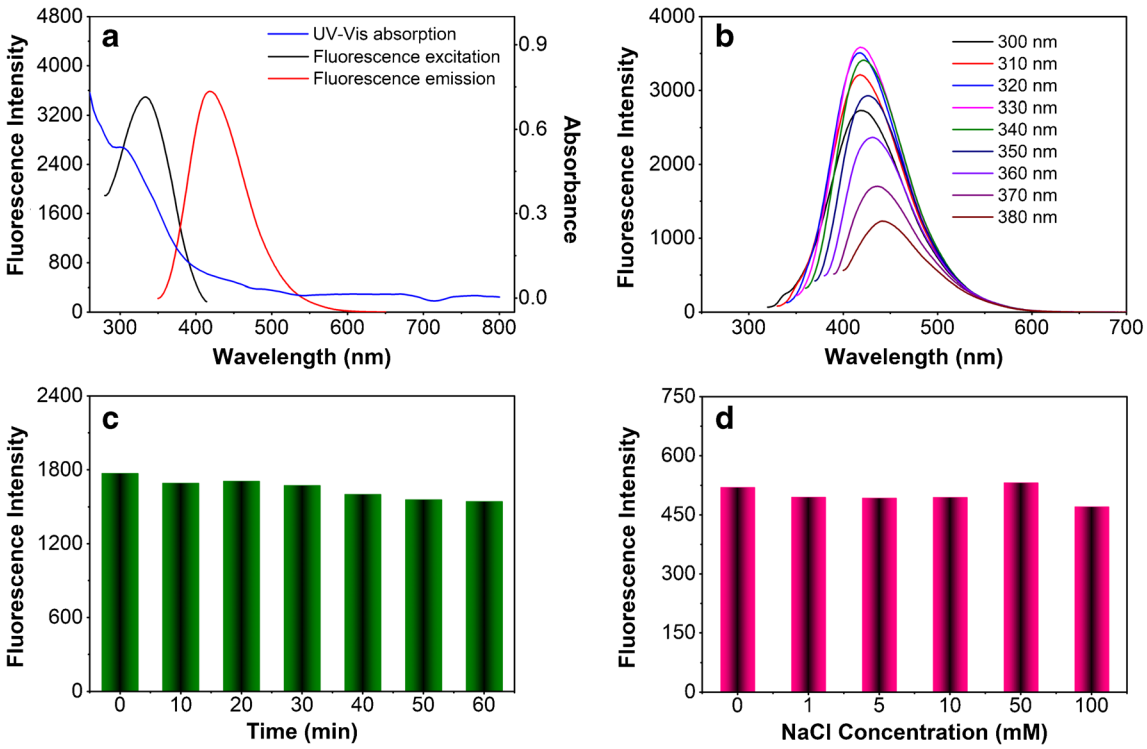

Fig. 3 Optical properties of SiNPs. **a** Spectra of UV-Vis absorption, fluorescence excitation, and fluorescence emission. **b** Fluorescence emission spectra at different excitation wavelengths. **c** Fluorescence stability against photobleaching. **d** Salt tolerance performance

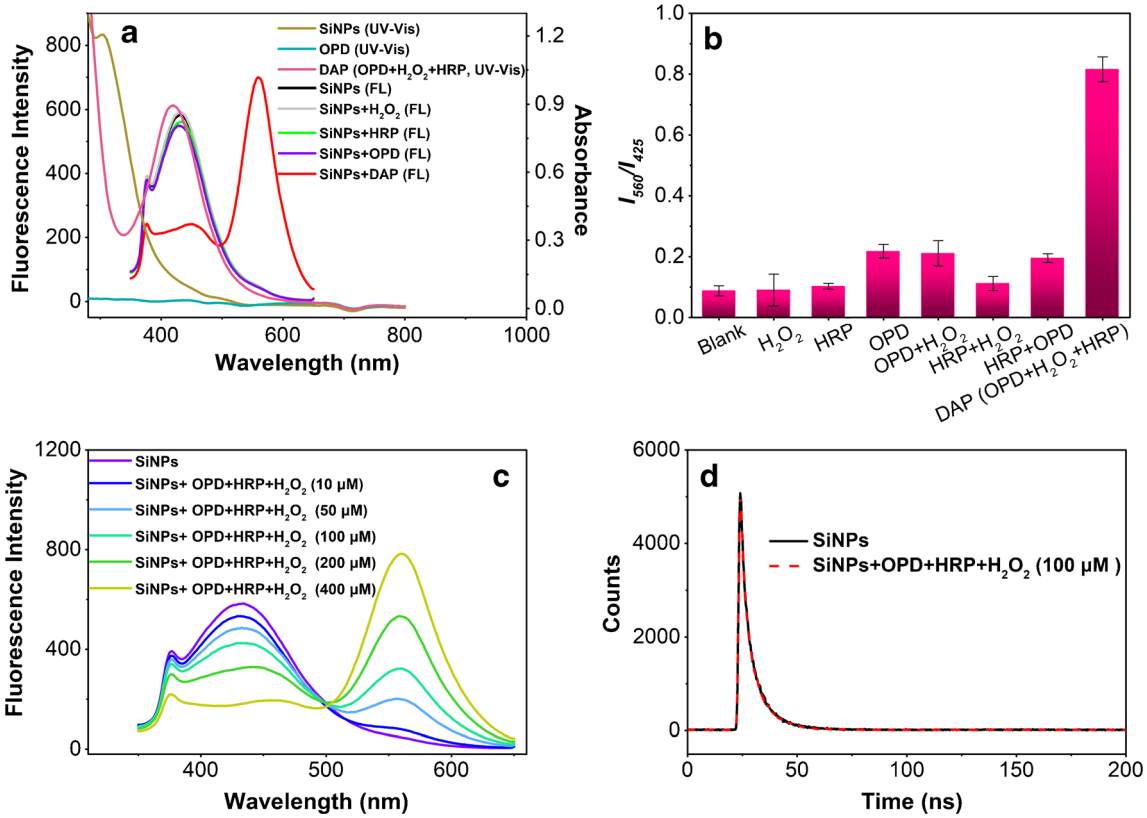

Fig. 4 **a** UV-Vis absorption spectra of SiNPs, OPD, and DAP, and fluorescence emission spectra of SiNPs coexisting with HRP, OPD, or DAP. **b** Ratiometric fluorescence responses of SiNPs with different substrates. **c** Fluorescence emission spectra of SiNPs in the presence of DAP. **d** Fluorescence lifetime of SiNPs in the presence or absence of DAP. Concentrations of OPD and HRP are 20 mM and 0.5 mg/mL, respectively

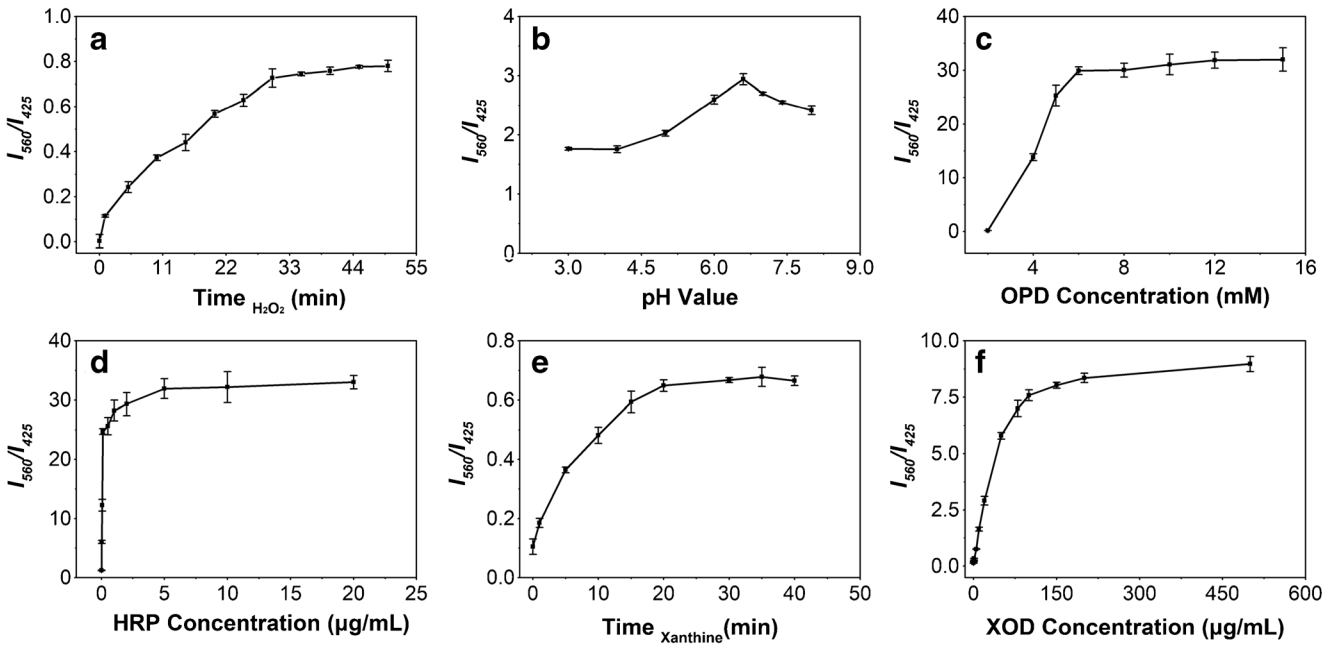

Fig. 5 Optimization of analytical conditions for sensing H_2O_2 or xanthine, including **a** incubation time for sensing H_2O_2 and **b** pH value, **c** incubation temperature, **d** concentration of OPD, **e** concentration of HRP, **f** incubation time, and **g** concentration of XOD for sensing xanthine

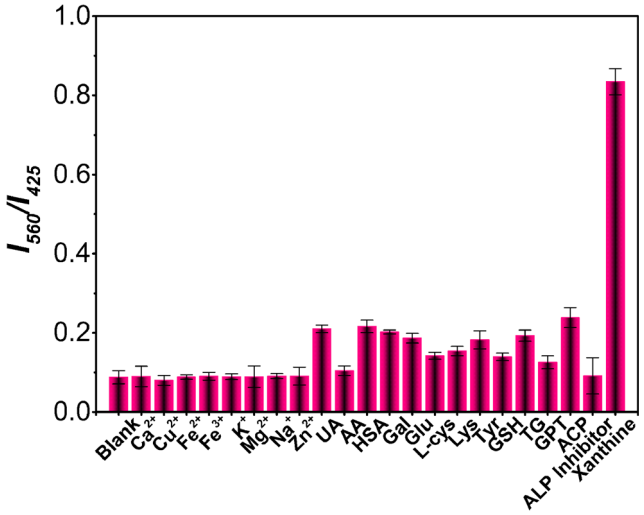

Fig. 6 Selectivity investigation of the present assay towards xanthine using real human serum as matrix. The spiked concentration of xanthine was 100 μM. Spiked concentrations of L-Cys, Lys, Tyr, GSH, ACP, and TG were 13.75 mg/L. The spiked concentration of HSA was 5 mg/mL. Spiked concentrations of ALP inhibitor (Na_3VO_4) and GPT were 0.5 mM and 10 U/L, respectively. Spiked concentrations of AA, UA, Gal, and Glu were 13.75 mM. The concentration of each inorganic ion was 275 μM

Next, the roles of the IFE and static quenching effect (SQE) in the quenching mechanism were evaluated. An equation (Eq. 1) for correcting the IFE in fluorescence spectra was employed to restore the ideal fluorescence emission intensities of SiNPs at 425 nm without the influence of DAP [31].

$$\frac{F_{cor}}{F_{obsd}} = \frac{2.3dA_{ex}}{1-10^{-dA_{ex}}} \cdot 10^{gA_{em}} \cdot \frac{2.3sA_{em}}{1-10^{-sA_{em}}} \quad (1)$$

where F_{cor} is the corrected fluorescence intensity, in which the IFE has been corrected; F_{obsd} is the observed fluorescence intensity; and A_{ex} and A_{em} are the absorbance values at the peak wavelengths of fluorescence excitation and emission (330 nm and 425 nm), respectively. As exhibited in ESM Fig. S1, d and s represent the width of the sample cuvette ($d = 1.0$ cm) and the thickness of the excitation light beam ($s = 0.1$ cm), and g is the distance between the edge of the excitation light beam and the edge of the sample cuvette ($g = 0.4$ cm) [32]. The correction factor (CF) for the IFE of DAP on the fluorescence of the SiNPs and the quenching efficiencies (E_{obsd} and E_{cor}) based on the observed and the corrected fluorescence intensities were also calculated, respectively. The results of the correction are listed in ESM Table S2. ESM Fig. S2 illustrates the variation in the fluorescence intensities (F_{obsd} and F_{cor}, a) and quenching efficiencies (E_{obsd} and E_{cor}, b) before and after correction. From these results, it was found that with the increased concentration of DAP, F_{obsd} decreased significantly while F_{cor} varied very little around its average value. Additionally, large ratios (~100% at

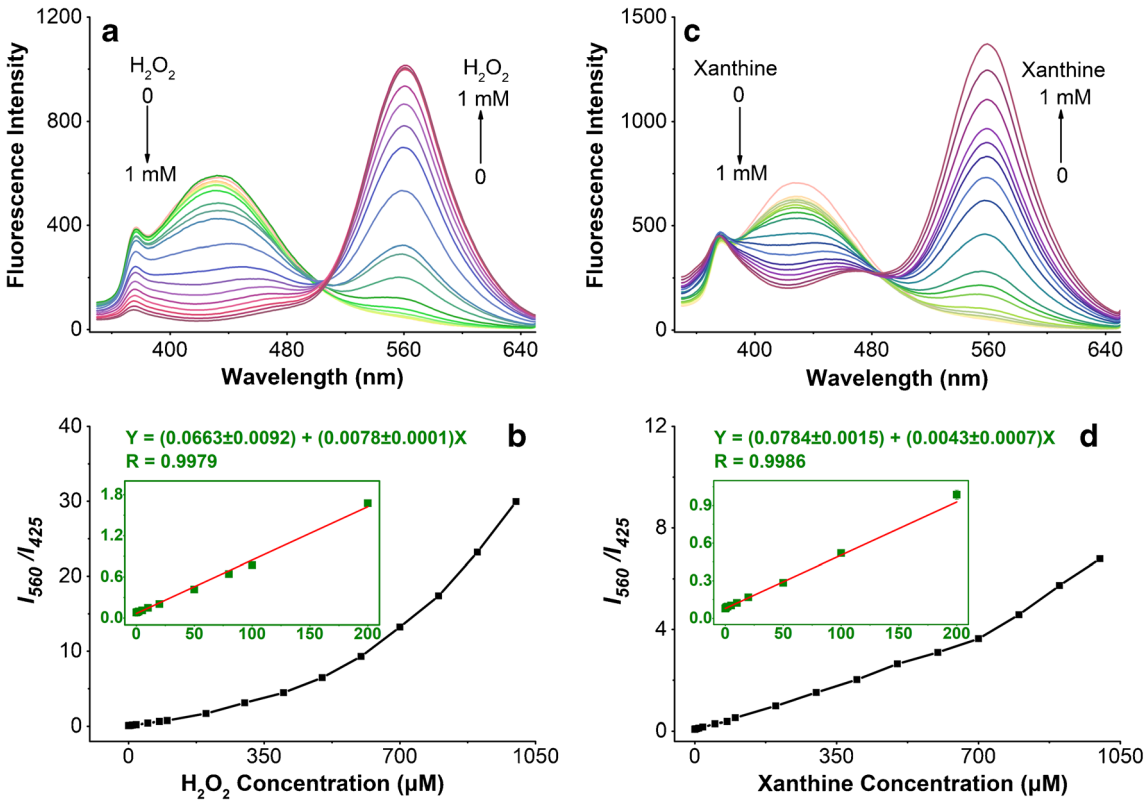

Fig. 7 Fluorescence responses of the present assay towards **a** H_2O_2 and **c** xanthine, and calibration lines for detecting **b** H_2O_2 and **d** xanthine

a DAP concentration of 10 μM) of the IFE-induced quenching efficiency (E_{obsd} - E_{cor}) to the total quenching efficiency (E_{obsd}) were obtained. The F_{cor} values larger than $F_{cor,\ 0}$ (F_{cor} value in the absence of DAP) and E_{cor} values less than zero may be ascribed to the slight response fluctuation of the instruments. These results indicate the dominant role of the IFE in the quenching mechanism.

According to the Stern–Volmer equation (Eq. 2), which is usually employed for describing the SQE of the quencher on fluorophores, in this work the ratio of corrected fluorescence intensity in the absence of DAP to that in the presence of DAP ($F_{cor,\ 0}$ / F_{cor}) exhibited a linear response to the concentration of DAP ([*Q*]), with a positive slope (K_{sv}) if SQE contributed to the process of fluorescence quenching.

$$\frac{F_0}{F} = 1 + K_{SV}[Q] \tag{2}$$

However, as shown in ESM Fig. S2c, the slope of the above linear response (if it existed) was near zero, revealing that the SQE was negligible in the quenching process.

Based on the above investigations, the IFE of DAP on the fluorescence emission of SiNPs was confirmed as the quenching mechanism of the present assay.

Optimization of analytical conditions

Several experimental parameters affecting the analytical performance of this assay were investigated, including the length of incubation time, the pH value of the PB solution, and the concentrations of PPD, HRP, and XOD. Based on the temperature requirement for enzyme-catalyzed oxidation reactions in the human body, 37 °C was selected as the incubation temperature for the assay. As suggested in Fig. 5a, the oxidation reaction of PPD reached equilibrium after incubation for 30 min. Hence, an incubation time of 30 min was chosen for subsequent measurement of H_2O_2. The results presented in Fig. 5b indicate that the optimal pH value for this assay was 6.6. The concentrations of OPD and HRP were also optimized to obtain a satisfactory dynamic detection range. According to the results as illustrated in Fig. 5c and d, the concentrations of OPD and HRP were respectively set at 20 mM and 0.5 mg/mL in subsequent experiments.

The incubation time and the concentration of XOD for the oxidation reaction of xanthine were also studied. An incubation time of 30 min and a XOD concentration of 0.2 mg/mL were finally chosen as the optimal conditions for subsequent determination of xanthine based on the results shown in Fig. 5e and f.

Selectivity

The interference of common inorganic ions (K^+, Na^+, Mg^{2+}, Ca^{2+}, Fe^{2+}, Fe^{3+} Cu^{2+}, and Zn^{2+}), ALP inhibitor (Na_3VO_4), and biomolecules (UA, AA, HSA, Glu, Gal, Tyr, TG, L-Cys, Lys, GSH, GPT, and ACP) which might coexist with xanthine in real serum samples was evaluated. As displayed in Fig. 6, no obvious influence induced by inorganic ions and only very slight interference of several biomolecules was observed, indicating the good selectivity of this assay for xanthine.

Sensing of H_2O_2

The fluorescence response of this assay towards H_2O_2 is shown in Fig. 7a. Under the optimal analytical conditions, it is obvious that a gradual enhancement of fluorescence emission of DAP at 560 nm and an associated decay of fluorescence emission at 425 nm occurred with the increasing concentration of H_2O_2. Figure 7b shows the plots of ratiometric fluorescence values (I_{560}/I_{425}) versus the concentrations of H_2O_2. A limit of detection (LOD) of 0.05 μM for H_2O_2 was obtained by calculating the concentration of target analyte giving the response signal equal to three times the standard deviation (3σ) of the blank signals.

Sensing of xanthine

The fluorescence response of this assay towards xanthine was also measured (Fig. 7c). The trend in the fluorescence variation of DAP at 560 nm and that of the SiNPs at 425 nm with

Table 1 Comparison of the analytical performance of the proposed assay with other reported methods for xanthine detection

Method	Brief description of process for preparation of probe or determination	Testing time (min)	Linear range (μM)	LOD (μM)
HPLC-UV [3, 8]	Complex sample pretreatment procedure, including precipitation, adding internal standard, drying, vortexing, centrifuging, filtering	>50	1–100 or 0.2–20	0.12
Colorimetry [6]	Long-time and complex synthesis of WO_3 nanosheets	60	25–200	1.24
Colorimetry [34]	Simple synthesis of $MoSe_2$ nanosheets	20	10–320	1.96
Electrochemistry [4]	Modified edge-plane pyrolytic graphite electrode for each sample	4	0.1–50	0.06
Ratiometric fluorometry [10]	N/Cu-co-doped CDs	31	0.25–75	0.10
Surface plasma resonance [9]	Complex synthesis procedure for XO-modified Ta_2O_5 nanofibers	1	0–3	0.013
Ratiometric fluorometry (this work)	One-pot synthesis of SiNPs without doping	30	0.3–200	0.11

Table 2 Detection results for xanthine in real and spiked human serum samples by the proposed assay and a reference HPLC method ($n = 3$)

Human serum	Spiked (μM)	This assay			Reference HPLC method		
		Detected (μM)	Recovery (%)	RSD (%)	Detected (μM)	Recovery (%)	RSD (%)
Sample 1	0	9.65	–	4.0	9.83	–	3.2
	10	18.8	91.9	1.5	19.8	99.3	5.9
	50	58.5	97.6	2.0	61.0	102.3	2.5
Sample 2	0	13.8	–	5.1	13.3	–	1.9
	10	23.2	93.6	1.5	23.0	97.3	3.4
	50	63.2	98.7	1.9	62.2	97.8	4.5
Sample 3	0	1.28	–	5.5	1.35	–	3.7
	10	11.3	100.2	3.7	11.3	99.5	2.4
	50	51.2	99.9	5.0	51.8	100.9	6.0

the increasing concentration of xanthine (Fig. 7d) are similar to those exhibited during the sensing of H_2O_2 (Fig. 7b), since the total amount of H_2O_2 generated during the oxidation of xanthine is dependent on the total amount of xanthine in the testing sample. By a similar calculation as in Section 3.5, a low LOD for xanthine of 0.11 μM was obtained by the present assay, which is far lower than the normal xanthine concentration range in healthy human plasma (0.5–2.5 μM) or urine (40–160 μM) [33].

The analytical performance of the solo DAP fluorescence-based assay was evaluated (ESM Fig. S3) for comparison. The LODs of H_2O_2 and xanthine obtained by this simplified assay were 1.01 μM and 1.28 μM, respectively. The present ratiometric fluorescence assay thus demonstrates superiority over the solo DAP fluorescence-based assay, with much lower LOD values, wider linear ranges, and better stability against the response fluctuations of instruments.

A comparison of the analytical performance of the proposed assay with other reported methods for sensing xanthine is presented in Table 1. The results further demonstrate the advantages of the proposed assay, including the simple preparation and excellent storage stability of the fluorescent material, facile fabrication and application of the testing platform, good sensitivity, and wide linear range.

Sensing of xanthine in human serum samples

The applicability of the proposed assay was tested by quantifying xanthine in both real and spiked human serum samples. Xanthine concentrations in all samples were verified by a reference method using high-performance liquid chromatography (HPLC) [3]. Good recovery efficiency in the range of 91.9%–100.2% was obtained by the proposed assay, with relative standard deviations (RSDs) ranging from 1.5% to

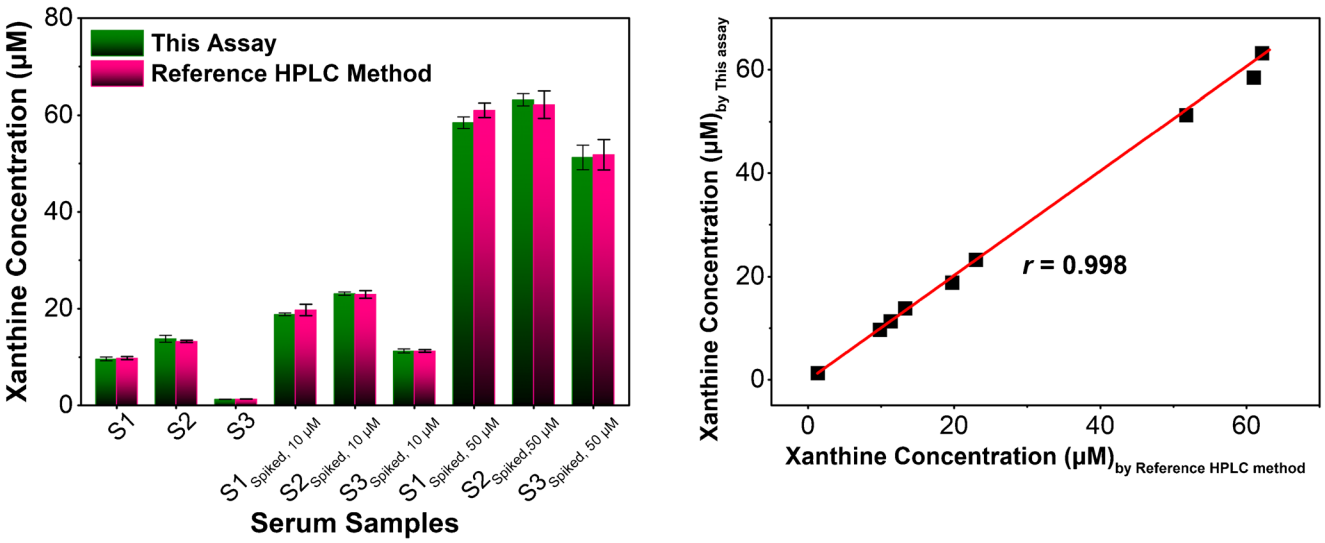

Fig. 8 **a** Comparison and **b** correlation of the detection results for xanthine in real and spiked human serum samples obtained by the proposed assay and a reference HPLC method

5.5% (Table 2). Moreover, the total run time for the assay, which consists mainly of the incubation period, is little more than 30 min even in batch mode. A correlation coefficient (r) of 0.998 was calculated for the results obtained by these two methods (Fig. 8). These results show the promise of the proposed assay for application in rapid clinical diagnostics.

Conclusions

In this work, a sensitive ratiometric fluorescence assay was proposed for sensing xanthine in human serum based on the fluorescence emission of DAP and the IFE of DAP on the fluorescence emission of SiNPs. Two continuous enzyme-catalyzed oxidation reactions linked by the generation and consumption of H_2O_2 were employed to produce DAP in an amount proportional to the amount of xanthine in the sample. The striking analytical performance obtained demonstrated the excellent applicability of this assay. Compared with other reported approaches, two advantages of the proposed assay deserve to be mentioned. First, the SiNP material, prepared by a novel and facile technique providing a superior fluorescence quantum yield (~16%), was applied to the assay directly without further chemical modification or labeling to manipulate or improve its fluorescence behavior, which greatly facilitated the fabrication and improved the sensitivity of the proposed assay. Second, by mixing all the reaction reagents with the serum sample in a single step for the continuous enzyme-catalyzed oxidation reactions, the total running time of this assay was shortened significantly. The proposed assay demonstrates great potential for further application in disease diagnostics and bioanalysis, especially for the detection of biological metabolites involved in H_2O_2 generation or consumption reactions.

Supplementary Information The online version contains supplementary material available at https://doi.org/10.1007/s00216-020-03104-7.

Acknowledgements This work was supported by the State Scholarship Fund of China (No. 201806175003), Industrialization Project of the Education Department of Jilin Province of China (No. JJKH20200944KJ), the National Natural Science Foundation of China (31771093), the Project of International Collaboration of Jilin Province (201180414085GH), the Fundamental Research Funds for the Central Universities, the Program for JLU Science and Technology Innovative Research Team (2017TD-27, 2019TD-36), and "The 13th Five-Year" industrialization project of Jilin Education Department (JJKH20190109KJ, 2019C023, 2018SCZ038).

Compliance with ethical standards

All applicable international, national, and/or institutional guidelines for the collection and use of human blood and serum samples were followed.

Human ethics The study was approved by the Institutional Ethics Committee of China-Japan Union Hospital of Jilin University, Changchun, China (No. 2019040811).

Conflict of interest The authors declare that there is no conflict of interest regarding the publication of this article.

References

1. Luo A, Lian Q, An Z, Li Z, Guo Y, Zhang D, et al. Simultaneous determination of uric acid, xanthine and hypoxanthine based on sulfonic groups functionalized nitrogen-doped graphene. J Electroanal Chem. 2015;756:22–9.
2. Bas SZ, Gulce H, Yildiz S, Gulce A. Amperometric biosensors based on deposition of gold and platinum nanoparticles on polyvinylferrocene modified electrode for xanthine detection. Talanta. 2011;87:189–96.
3. Wang Y, Deng M, Deng B, Ye L, Fei X, Huang Z. Study on the diagnosis of gout with xanthine and hypoxanthine. J Clin Lab Anal. 2019;33(5):e22868.
4. Pierini GD, Robledo SN, Zon MA, Di Nezio MS, Granero AM, Fernández H. Development of an electroanalytical method to control quality in fish samples based on an edge plane pyrolytic graphite electrode. Simultaneous determination of hypoxanthine, xanthine and uric acid. Microchem J. 2018;138:58–64.
5. Dervisevic M, Dervisevic E, Cevik E, Senel M. Novel electrochemical xanthine biosensor based on chitosan-polypyrrole-gold nanoparticles hybrid bio-nanocomposite platform. J Food Drug Anal. 2017;25(3):510–9.
6. Li Z, Liu X, Liang XH, Zhong J, Guo L, Fu F. Colorimetric determination of xanthine in urine based on peroxidase-like activity of WO_3 nanosheets. Talanta. 2019;204:278–84.
7. Bory C, CC RB. Comparison of capillary electrophoretic and liquid chromatographic determination of hypoxanthine and xanthine for the diagnosis of xanthinuria. J Chromatogr A. 1996;730:329–31.
8. Cooper N, Khosravan R, Erdmann C, Fiene J, Lee JW. Quantification of uric acid, xanthine and hypoxanthine in human serum by HPLC for pharmacodynamic studies. J Chromatogr B Anal Technol Biomed Life Sci. 2006;837(1–2):1–10.
9. Kant R, Tabassum R, Gupta BD. Xanthine oxidase functionalized Ta_2O_5 nanostructures as a novel scaffold for highly sensitive SPR based fiber optic xanthine sensor. Biosens Bioelectron. 2018;99:637–45.
10. Ma Y, Cen Y, Sohail M, Xu G, Wei F, Shi M, et al. A ratiometric fluorescence universal platform based on N, Cu codoped carbon dots to detect metabolites participating in H_2O_2-generation reactions. ACS Appl Mater Interfaces. 2017;9(38):33011–9.
11. Menon S, Girish Kumar K. A fluorescent biosensor for the determination of xanthine in tea and coffee via enzymatically generated uric acid. LWT. 2017;86:8–13.
12. Zhang H, Chen Y, Liang M, Xu L, Qi S, Chen H, et al. Solid-phase synthesis of highly fluorescent nitrogen-doped carbon dots for sensitive and selective probing ferric ions in living cells. Anal Chem. 2014;86(19):9846–52.
13. Qian Z, Chai L, Tang C, Huang Y, Chen J, Feng H. Carbon quantum dots-based recyclable real-time fluorescence assay for alkaline phosphatase with adenosine triphosphate as substrate. Anal Chem. 2015;87(5):2966–73.
14. Peng F, Su Y, Zhong Y, Fan C, Lee S, He Y. Silicon nanomaterials platform for bioimaging, biosensing, and cancer therapy. Acc Chem Res. 2014;47(2):612–23.
15. Folarin E, Yong KT, Roy I, Hu R, Law WC, Zhao WW, et al. In vivo targeted cancer imaging, sentinel lymph node mapping and multi-channel imaging with biocompatible silicon nanocrystals. ACS Nano. 2011;5(1):413–23.
16. Li Q, Luo TY, Zhou M, Abroshan H, Huang J, Kim HJ, et al. Silicon nanoparticles with surface nitrogen: 90% quantum yield

with narrow luminescence bandwidth and the ligand structure based energy law. ACS Nano. 2016;10(9):8385–93.
17. Yi Y, Zhu G, Liu C, Huang Y, Zhang Y, Li H, et al. A label-free silicon quantum dots-based photoluminescence sensor for ultrasensitive detection of pesticides. Anal Chem. 2013;85(23):11464–70.
18. Li D, Jiang Y, Chen S, Zhao Q, Zhang Y, Wang W, et al. A simple and sensitive assay of alkaline phosphatase activity in serum by fluorescent silicon nanoparticles based on inner filter effect. Sensors Actuators B Chem. 2020;307:127589.
19. Chen S, Yu YL, Wang JH. Inner filter effect-based fluorescent sensing systems: a review. Anal Chim Acta. 2018;999:13–26.
20. Han Y, Chen Y, Feng J, Liu J, Ma S, Chen X. One-pot synthesis of fluorescent silicon nanoparticles for sensitive and selective determination of 2,4,6-trinitrophenol in aqueous solution. Anal Chem. 2017;89(5):3001–8.
21. Wu F, Zhang X, Kai S, Zhang M, Wang H, Myers JN, et al. One-step synthesis of superbright water-soluble silicon nanoparticles with photoluminescence quantum yield exceeding 80%. Adv Mater Interfaces. 2015;2(16):1500360.
22. Song W, Duan W, Liu Y, Ye Z, Chen Y, Chen H, et al. Ratiometric detection of intracellular lysine and pH with one-pot synthesized dual emissive carbon dots. Anal Chem. 2017;89(24):13626–33.
23. Nsanzamahoro S, Mutuyimana FP, Han Y, Ma S, Na M, Liu J, et al. Highly selective and sensitive detection of catechol by one step synthesized highly fluorescent and water-soluble silicon nanoparticles. Sensors Actuators B Chem. 2019;281:849–56.
24. Han Y, Chen Y, Feng J, Na M, Liu J, Ma Y, et al. Investigation of nitrogen content effect in reducing agent to prepare wavelength controllable fluorescent silicon nanoparticles and its application in detection of 2-nitrophenol. Talanta. 2019;194:822–9.
25. Ma SD, Chen YL, Feng J, Liu JJ, Zuo XW, Chen XG. One-step synthesis of water-dispersible and biocompatible silicon nanoparticles for selective heparin sensing and cell imaging. Anal Chem. 2016;88(21):10474–81.
26. Chen X, Zhang X, Xia LY, Wang HY, Chen Z, Wu FG. One-step synthesis of ultrasmall and ultrabright organosilica nanodots with 100% photoluminescence quantum yield: long-term lysosome imaging in living, fixed, and permeabilized cells. Nano Lett. 2018;18(2):1159–67.
27. Zhang M, Su R, Zhong J, Fei L, Cai W, Guan Q, et al. Red/orange dual-emissive carbon dots for pH sensing and cell imaging. Nano Res. 2019;12(4):815–21.
28. Wang X, Cao L, Yang ST, Lu F, Meziani MJ, Tian L, et al. Bandgap-like strong fluorescence in functionalized carbon nanoparticles. Angew Chem Int Ed Engl. 2010;49(31):5310–4.
29. Sharma B, Tanwar S, Sen T. One pot green synthesis of Si quantum dots and catalytic Au nanoparticle–Si quantum dot nanocomposite. ACS Sustain Chem Eng. 2019;7(3):3309–18.
30. Liu J, Chen Y, Wang W, Feng J, Liang M, Ma S, et al. "Switch-on" fluorescent sensing of ascorbic acid in food samples based on carbon quantum dots-MnO_2 probe. J Agric Food Chem. 2016;64(1):371–80.
31. Gauthier TD, Shane EC, Guerin WF, Rudolf Seitz W, Grant CL. Fluorescence quenching method for determining equilibrium constants for polycyclic aromatic hydrocarbons binding to dissolved humic materials. Environ Sci Technol. 1986;20:1162–6.
32. Kubista M, Sjoback R, Eriksson S, Albinsson B. Experimental correction for the inner-filter effect in fluorescence spectra. Analyst. 1994;119:417–9.
33. Boulieu R, Bory C, Baltassat P, Gonnet C. Hypoxanthine and xanthine levels determined by high-performance liquid chromatography in plasma, erythrocyte, and urine samples from healthy subjects: the problem of hypoxanthine level evolution as a function of time. Anal Biochem. 1983;129(2):398–404.
34. Wu X, Chen T, Wang J, Yang G. Few-layered $MoSe_2$ nanosheets as an efficient peroxidase nanozyme for highly sensitive colorimetric detection of H_2O_2 and xanthine. J Mater Chem B. 2018;6(1):105–11.

Publisher's note Springer Nature remains neutral with regard to jurisdictional claims in published maps and institutional affiliations.